17th World Conference on Earthquake Engineering, 17WCEE
Sendai, Japan - September 13th to 18th 2020

CONTINUOUS SEISMIC MONITORING OF SEISMICALLY ISOLATED CABLE-STAYED BRIDGE BY WIRELESS SENSOR NETWORK

D. M. Siringoringo(1), Y. Fujino(2),V. Mehta(3), M.Suzuki(4)

(1) *Assoc. Prof., Institute of Advanced Sciences, Yokohama National University, dion@ynu.ac.jp*
(2) *Dist. Prof., Institute of Advanced Sciences, Yokohama National University, fujino@ynu.ac.jp*
(3) *Graduate Student, Dept. of Urban Innovation, Yokohama National University, mehta-vaibhav-rx@ynu.jp*
(4) *Sonas Corp., makoto@sonas.co.jp*

Abstract

Developments of structural monitoring using wireless sensor network for large-scale civil structures have been very active in recent years. Numerous models and applications of wireless sensors network have been developed and implemented in laboratory-scale experiment or full-scale deployment. This paper describes an ongoing research work on the seismic monitoring of cable-stayed bridge using wireless sensor network. Newly developed wireless sensor network that is based on simultaneous high-speed flooding technique was implemented on the Shin-Nakagawa Bridge, a 530-m single-plane single-pylon steel-box girder cable-stayed bridge in Ibaraki prefecture, Japan. The structure is seismically isolated with rubber bearings and damper at the main pylon and piers. The bridge was damaged by the 2011 Great East Japan (Tohoku) Earthquake. Fracture and cracks of the rubber were observed on several parts of laminated rubber bearing above the main tower. After the earthquake, the damaged parts were fixed and the bridge was retrofitted by adding oil damper at the connection between girder and main tower, and uplifting prevention device. As a part of monitoring, a total of 26 wireless sensor nodes were installed on the cable-stayed bridge and viaduct at several locations on the pier, main pylon, girder and on the ground. The monitoring system has been in place since 2017 and successfully recorded structural responses from more than 30 small-to-moderate scale earthquakes until February 2020. This paper describes the wireless sensor network system, the scheme for monitoring system and analysis of recorded earthquakes.

Keywords: seismic monitoring, wireless sensors, cable-stayed bridge, seismically isolated bridge, system identification

1. Introduction

Developments of structural monitoring using wireless sensor network (WSN) for large-scale civil structures have been very active in recent years [1,2]. Numerous models and applications of wireless sensors network have been developed and implemented in laboratory-scale experiment or full-scale deployment on structures. While, deployments of wireless sensors for ad-hoc monitoring campaign for short-term and long-term duration using ambient and wind-induced vibrations been attempted in various research works in the past [3,4,5,6]; deployment of wireless sensors for continuous long-term monitoring of seismic responses is not yet common.

In this paper, we describe an ongoing work on the seismic monitoring of cable-stayed bridge using WSN. The newly developed WSN that is based on simultaneous high-speed flooding technique is found efficient in transmitting the packets at the same time without causing synchronization problem to the carrier's frequency or phase [7]. The technique allows for a stable and highly efficient sensor network. This paper describes the sensing system, implementation of the monitoring system, and data analysis using information from seismic responses recorded by the wireless sensing network.

2. Description of the Cable-Stayed Bridge

The object of monitoring is Shin-Nakagawa Bridge located at the suburb of Mito City, Ibaraki Prefecture, east of Japan (Fig. 1). It is a single-plane single tower cable-stayed bridge with the total span length 533 m and width of 22m. The superstructure consists of continuous steel box girder; the longest span is 283.9m crossing over the Nakagawa river and three-continuous side spans of 113m, 75m, and 58.9m supported by three piers. The bridge is supported by fifteen stay cables arranged in a harp configuration, radiating from the main tower 50.4m above the deck.

The substructure consists of four reinforced concrete piers named P31, P32, P33, P34 and P35. Only P35 is located on the left bank of the Nakagawa River, while all other piers are located on the right bank of the Nakagawa River. The main tower (P34) is in the middle with the height 127.5m. All piers are supported by pile foundation while the main tower is supported by caisson foundation. The bridge was opened in 1997 and became a part of the East Mito route highway.

Fig. 1 – Shin-Nakagawa cable-stayed bridge (36°21'25.81"N, 140°33'28.04"E).

The bridge was designed using seismic code prior to the 1995 Kobe earthquake. The bridge was damaged during the 2011 Great East Japan (Tohoku) earthquake. Fracture and cracks of the rubber were observed on several parts of the laminated rubber bearing located on P31, P34 and P35 [8]. The upper bearing of P35 on the upstream side was broken because the earthquake-induced displacement exceeded the allowable deformation and the girder collided with the approach span on the Katsuta viaduct side. The longitudinal displacement of the girder at the main tower also exceeded the limit and caused damages on the bolts and rubber layer of the laminated rubber bearing. In addition, although all bearings on pier P32 and P33 showed evidence of crushing of the mortar and pounding of the side block and the upper rod, there was no significant damage to the rubber bearings’ main body on these piers. After the earthquake, the damaged parts were fixed, and the bridge was retrofitted by adding oil damper at the connection between girder and main tower, and uplifting prevention device on the top of pier P35.

	Sensor	Noise levels	power consumption
EPSON M-A351AU		1μg / √Hz	20mA
Analog Devices ADXL355		25μg / √Hz	200μA

Fig. 2 – Wireless acceleration sensor node and specification) courtesy of SONASCO.LTD [7]

3. Wireless Sensor Network (WSN) System

In this study a WSN protocol called Choco is employed. The Choco protocol was developed using Concurrent Transmission Flooding (CTF) principle, with five main features and strategies required toward developing structural monitoring system [7]. These five main features are described in the following. 1) Low power consumption: battery life of several years with two D-cell batteries, power consumption of all operation including synchronization, sensor sampling, and storage were lower than several 100 mA. 2) Robust: the system is deployable even by those who are not professional of wireless communication and network. 3) Fast synchronization: synchronization among wireless sensors is needed for analyzing the measured acceleration waves. 4) Reliable Transmission: the system does not allow data losses. 5) High throughput: high throughput is required since acceleration sensors generate huge amount of data. Choco is a slotted communication protocol, and all communications are performed using CTF. The sink node in Choco works as a master node that coordinates communications of all the other nodes. The sink node periodically transmits time-synchronization packets to synchronize signal with the other nodes. Also, the sink node transmits the control packets to assign the slot owner. Only the node assigned as the slot owner can initiate a transmission, and the transmission is then forwarded by the non-owner nodes using CTF.

The scheduling of Choco is based on the backlog information from each node. Specifically, each node transmits backlog information in a packet header when it transmits a packet. The sink node continues to schedule new data transmission slots for the remaining packets or packet losses. Until there is no packet to be collected anymore, the sink node allows all other nodes to sleep by transmitting sleep packets which contain a wake-up time. When the wake-up time comes, all nodes wake up, and the sink node restarts the polling. When a node which has no packets is requested to send a packet, it transmits a null packet, which consists of only a packet header to inform the sink node of its zero backlog. When backlogs of all nodes are zero, the sink instructs all nodes to enter a sleep mode by sending sleep packets which include a wake-up time. On the wake-up time, the sink node considers all backlogs unknown. Choco can achieve synchronization, and robustness thanks to CTF [7].

Compared to routing-based communication, CTF-based one is more robust because it can use many paths concurrently. Choco can reduce overhead of idle listening because every node can sleep long time when there are no packets to be collected. Choco also achieves 100% reliable transport because the sink node continues to reschedule lost packets until the packets are delivered. Moreover, Choco achieves high throughput by continuously scheduling slots to nodes who have packets to be collected. The system provides a low-power sensor and a high-precision sensor from the perspective of precision, power consumption, and the existence of trigger function as described above. Analog Devices ADXL362, and EPSON M-A351AU are selected as a low-power sensor, and a high-precision sensor, respectively. Both sensors have a trigger function. The specification is summarized in Fig.2.

In implementation, sensor nodes can sleep almost all the time. Each 5ms, the power consumption rises to about 1 mA. This is due to CPU's activity of interrupt handling of timer compare. To generate a square wave whose cycle is 10 ms, the interrupt occurs each 5 ms. Every 31.25ms the power consumption rises to 2 mA. This is due to the activity of CPU and SRAM for reading and writing the measurements of an acceleration sensor. More details on the wireless sensor can be found in [7].

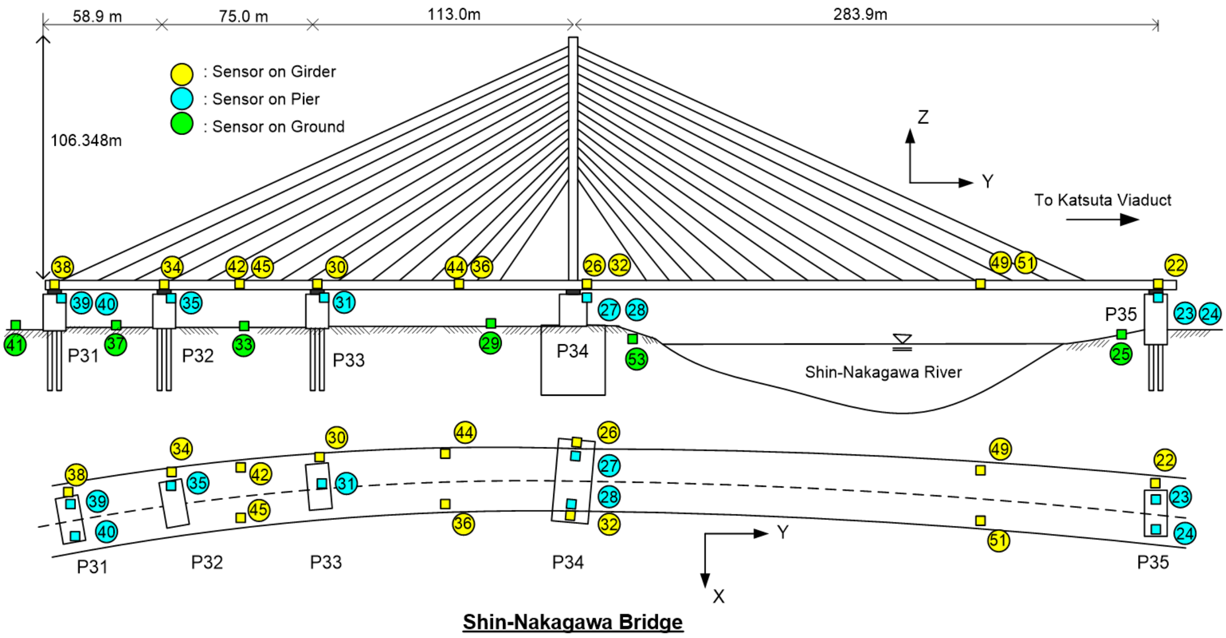

Fig. 3- Wireless sensor network on the Shin-Nakagawa cable-stayed bridge.

4. Deployment of Wireless Sensor Network System

A total 26 triaxial accelerometers were deployed on the bridge, consisting of 12 sensor nodes along the girder, 8 sensor nodes on the piers and 6 sensor nodes on the ground (Fig. 3). The pier sensors were placed on the top of pier caps at the same level as the isolator bearings. The girder sensors were placed on the side of the girder right above the isolator bearings. The arrangement is intended, among others, to evaluate performance of isolators during earthquake by taking the relative response between pier and girder. All sensors are arranged such that the x-axis measuring the bridge transversal vibration, y-axis measuring the bridge longitudinal vibration and z-axis for the vertical vibration.

The monitoring system was installed in summer 2017 and it has been recording seismic responses continuously since August 2017 until now (February 2020). The batteries need to be replaced every 6 months and at this time maintenance work is conducted. During the monitoring period between August 2017 and February 2020, the system has successfully recorded 35 seismic events, where majority of them are of small and moderate amplitudes.

Table 1 lists details of all recorded earthquakes that include far-field and near-field earthquakes. The three largest records (written in bold) are due to near-field earthquakes. Notable near-field earthquakes are on March 30th ,2018 (M5.1), July 17th,2018 (M4.8), June 17th,2019 (M5.1), and December 19th,2019 (M4.2), and January 21st,2020 (M4.3). Epicenter of all these near-field earthquakes are within 25km away from the bridge site. The monitoring system also successfully recorded several far-field earthquakes, with the farthest one was on February 13th, 2020, (M7.0) with the epicenter 1163km and away from the bridge site.

5. Description of Recorded Seismic Responses

In this section, we shall describe in more detailed responses from the two events, the largest recorded near-field earthquake July 17th, 2018 and the largest recorded far-field earthquake July 28th,2019. Fig. 4 shows examples of ground accelerations from node 41, 37 and 33 which were located on the near pier P31, P32 and P33 recorded from the largest recorded near-field earthquake on July 17th, 2018 and the largest recorded far-field earthquake on July 28th, 2019. For both earthquakes, the time-histories accelerations and frequency contents of the three ground nodes have nearly similar amplitude and characteristics in the three directions, suggesting similar type and conditions of soil along the bridge. Also noted the distinct large impulse at the beginning of the ground accelerations which are the common characteristics of nearfield earthquake ground motions, while for the far-field earthquake such large impulses do not appear.

Table 1 – Recorded Seismic Events by the WSN system at Shin-Nakagawa Bridge from 2017-2020

No.	Date	Epicenter [km]	Depth [km]	Magnitude [M]	Distance [km]	Peak Ground Acc.(PGA) [cm/s^2]
1.	11/3/2017	36.81N,140.53E	8	M4.8	50.41	64.7
2.	2/6/2018	36.63N,140.90E	51	M3.7	43.9	3.74
3.	3/25/2018	32.64N,140.89E	41	M5.8	414	1.26
4.	***3/30/2018***	***36.44N,140.62E***	***56***	***M5.1***	***10.95***	***121.8***
5.	5/17/2018	36.35N,140.60E	52	M5.3	75	6.14
6.	7/7/2018	35.16N,140.59E	57	M6.0	42	5.75
7.	***7/17/2018***	***36.43N,140.69E***	***52***	***M4.8***	***15***	***143.7***
8.	9/5/2018	36.48N,141.34E	60	M5.5	72	25.02
9.	11/27/2018	36.07N,139.86E	44	M5.0	75	6.22
10.	5/1/2019	36.27N,141.01E	42	M4.5	42	11.44
11.	5/25/2019	35.30N,140.3E	40	M5.1	120	2.27
12.	5/27/2019	36.70N,140.7E	10	M4.2	40.18	6.48
13.	***6/17/2019***	***36.50N,140.6E***	***80***	***M5.1***	***16.32***	***137.4***
14.	6/18/2019	38.60N,139.5E	10	M6.8	266	6.42
15.	7/17/2019	37.10N,141.6E	40	M4.4	124	1.58
16.	*7/20/2019*	*36.40N,140.8E*	*60*	*M3.6*	*22*	*7.15*
17.	7/25/2019	35.10N,140.6E	60	M5.3	140	1.45
18.	7/28/2019	33.00N,137.4E	420	M6.5	472	8.51
19.	7/29/2019	35.80N,141.0E	20	M4.6	74	5.39
20.	7/30/2019	32.90N,140.8E	60	M6.0	385	1.43
21.	8/4/2019	37.70N,141.7E	50	M6.2	181	19.04
22.	8/24/2019	37.40N,142.5E	25	M5.6	208	2.48
23.	12/4/2019	36.8N,140.6E	10	M4.8	49	28.6
24.	12/5/2019	36.8N,140.6E	10	M4.5	49	10.14
25.	12/11/2019	37.7N,141.9E	40	M5.2	191	3.5
26.	*12/19/2019*	*36.3N,140.7E*	*90*	*M4.2*	*14*	*22.20*
27.	1/3/2020	35.8N,141.2E	30	M5.9	85	40.79
28.	1/14/2020 (M)	36.1N,139.9E	50	M5.0	66	26.78
29	1/14/2020 (A)	36.1N,140.9E	50	M4.9	42	19.62
30	*1/21/2020*	*36.4N, 140.7E*	*50*	*M4.3*	*14*	*61.38*
31	2/1/2020 (1)	35.7N,140.7E	50	M5.1	74	5.30
32	2/1/2020 (2)	36.0N,140.1E	70	M5.3	57	23.57
33	2/6/2020	36.4N,141.6E	40	M5.6	93	6.85
34	2/12/2020	37.3N,141.4E	80	M5.5	129	15.15
35	2/13/2020	44.7N,148.9E	160	M7.0	1163	11.53

Note: Entries written in bold are the three largest recorded earthquakes. Entries written in Italic is the near-field earthquake; M: Mainshock, A: Aftershock.

About 3km to the east of the bridge there is a seismometer IBR007 within the KNET networks operated by National Research Institute for Earth Science and Disaster Resilience (NIED) [9]. The responses from IBR007 sensor was used to check the accuracy of responses recorded by WSN. Fig. 5 shows the comparison of acceleration response spectra between WSN (Node 41) and the triaxial seismometer of IBR007. The figures clearly shown that time-histories characteristics, namely, the arrival time of the P and S-wave, the peak and decay amplitude of the accelerations are very similar for both KNET IBR007 [9] sensor and WSN Node 41 for both seismic events. The acceleration response spectra also show a reasonably good agreement for between the responses recorded by period larger than 0.3s. Some discrepancies appear for lower period for near-field event which were thought to be attributed to the different soil characteristics between the one near the bridge and the one on the IBR007 sensor location. In general, the comparisons show that WSN ground sensor nodes accurately recorded the ground accelerations for both large intensity near-field earthquake and small intensity far-field earthquake.

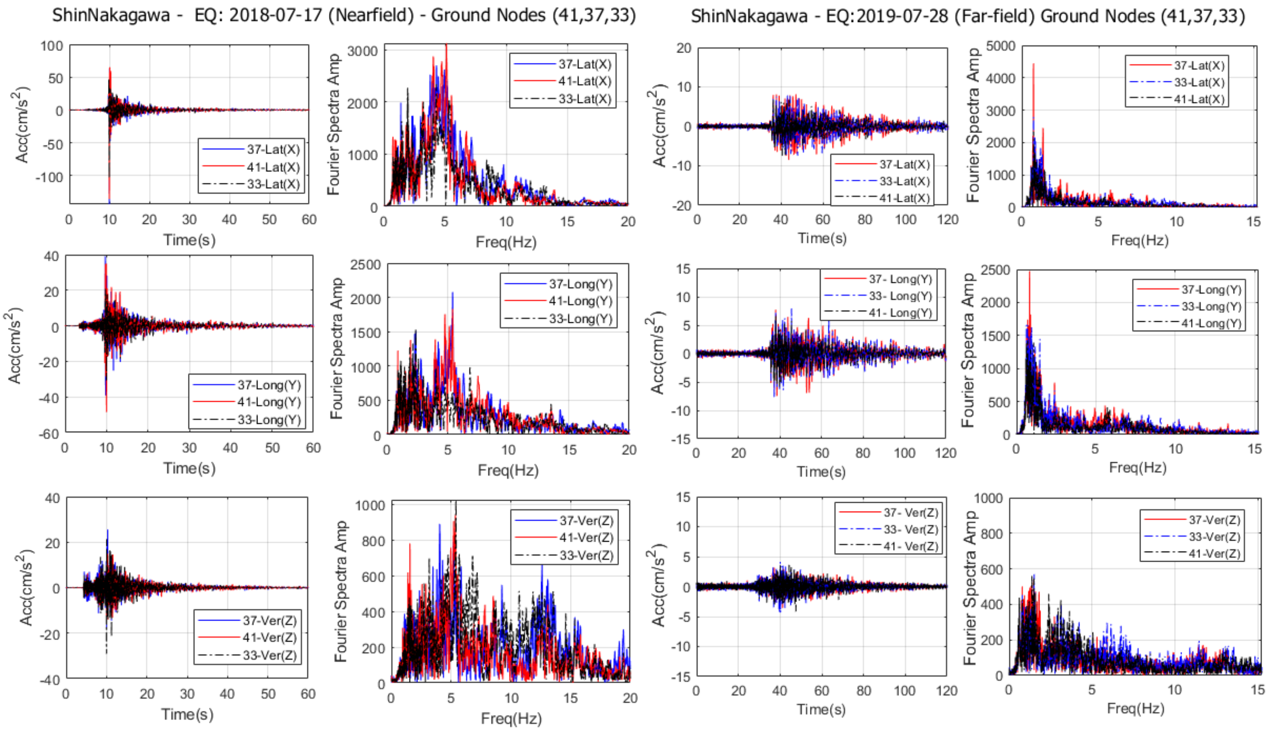

Fig. 4- Ground accelerations recorded by nodes on the free field during the nearfield largest earthquake (July 17^{th} ,2018) and far-field largest earthquake (July 28^{th} 2019).

5.1 Seismic Response of the Girder

The bridge girder is a continuous steel box resting on laminated rubber bearings and link or pendel bearings above the piers that accommodate longitudinal movement. Transversal movement of the girder is also expected although above the piers their displacements are limited by the lateral stopper. To avoid excessive longitudinal movement of the girder, viscous dampers located between main tower and girder were installed after 2011 Great East Japan (Tohoku) earthquake. Considering the girder configurations and characteristics, the longitudinal accelerations for all nodes along the girder are expected to be equal because the girder is a continuous steel box. Fig. 6 clearly demonstrates this evident. The longitudinal accelerations recorded by nodes 30, 44 and 51 are nearly the same for both near-field and far-field earthquakes, suggesting accuracy and reliability of the sensors in capturing structural vibration.

5.2. Seismic Response between Pier and the Girder

The bridge girder was supported by several types of bearings above the piers and at the main tower; namely; isolator laminated rubber bearings (LRB), wind shoes (WS), pendel bearing (PB), viscous damper (VD) and uplift prevention bearing (UP) as shown in detailed on Fig. 7. The support bearings accommodate longitudinal movement of the girder. Viscous dampers were placed between girder and the main tower to absorb vibration the girder in longitudinal direction. The lateral motion is limited by the wind shows, and possible uplift vertical motion at the end girder is prevented by the uplift prevention bearing at pier P35.

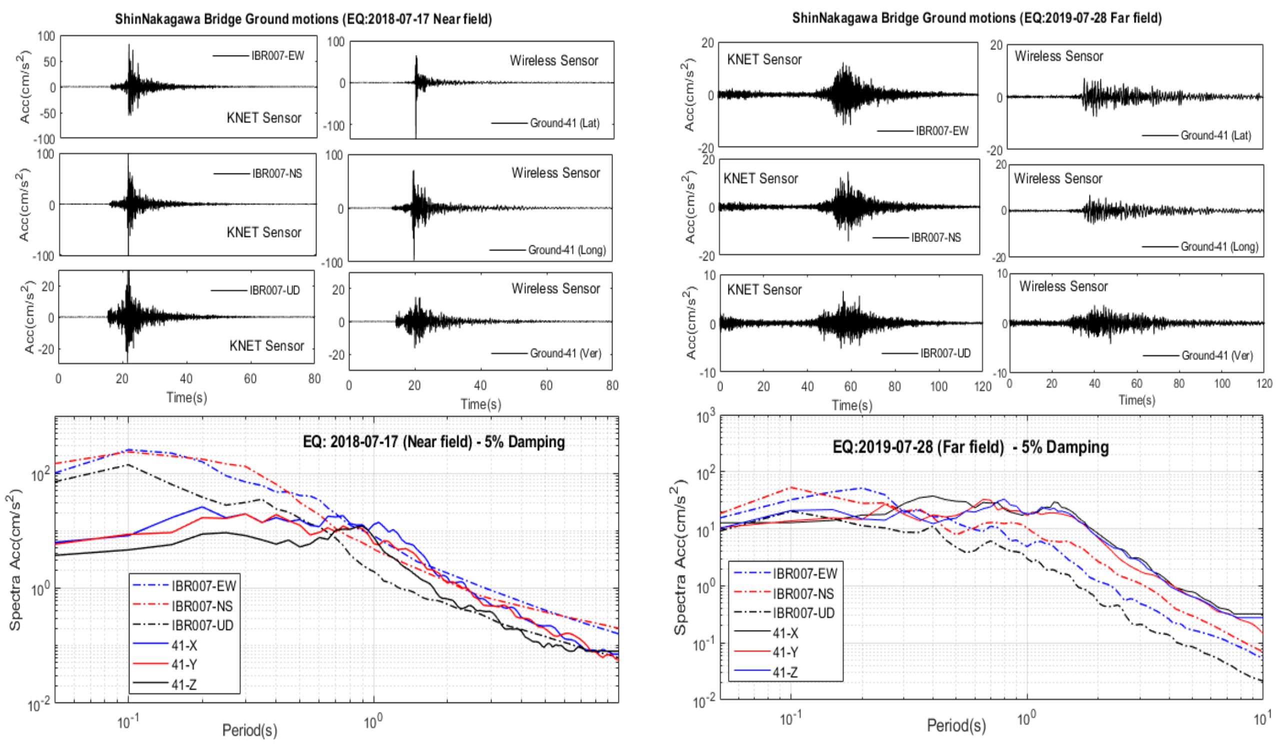

Fig. 5- Comparisons of ground accelerations recorded by nearby KNET IBR007 sensor and WSN Node 41 during the nearfield largest earthquake (July 17th ,2018) and far-field largest earthquake (July 28th 2019).

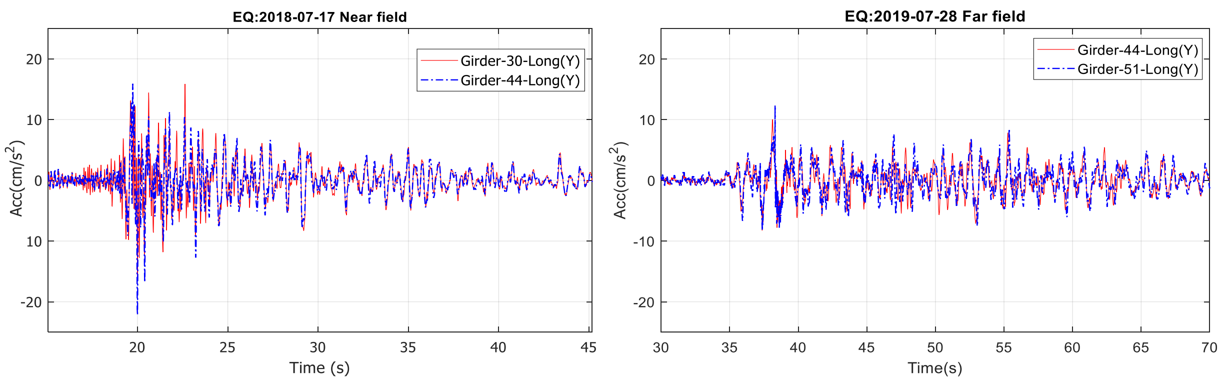

Fig. 6- Comparisons of longitudinal girder accelerations recorded by sensor nodes along the girder during the nearfield largest earthquake (July 17th ,2018) and far-field largest earthquake (July 28th 2019).

Performance of the isolators during an earthquake is essential to the overall bridge structural performance. The effectiveness of seismic isolators can be evaluated by whether they can successfully decouple the super-structure from the sub-structure. To capture such condition, sensors were placed on all pier caps and on the girder above the pier caps. With this arrangement, motion of the girder and pier cap were recorded and based on the records, performance of seismic isolators during earthquake can be evaluated.

Fig. 7-Types of bearings and vibration control devices between girder and piers

Time-histories and Fourier spectra of typical girder and top pier acceleration recorded during July 17th, 2018 earthquake are shown in Fig. 8. Note that the spectra of girder longitudinal accelerations, especially P32 and P33 contain the dominant super-structure's frequency while other frequencies of the pier cap record above 5Hz have been essentially filtered out. This indicates that the seismic isolation bearing has effectively decoupled the superstructure from the substructure. This demonstrates that in this earthquake, the seismic isolation system performed satisfactorily as indicted in previous study on the seismic behavior of isolated bridges [9,10].

6. Modal Parameters Identification using Seismic Responses

Using the recorded seismic response, one can evaluate behavior of the bridge and observe the trend in modal parameters with respect to the level of seismic excitation and their long-term characteristics. For this purpose, the state-of-the-art linear multi-input multi-output (MIMO) time-invariant system identification is utilized. It is a linear time domain system identification that utilizes input-output correlation matrix to estimate the coefficients of system state-space model. The algorithm allows identification from multiple source of excitation to accommodate the effect of varying ground motions at different supports that characterize seismic response of long-span bridge. The system identification algorithm utilizes correlation functions between input and output data to realize a state-space model and to estimate the modal parameters. The identification procedure starts by estimating the observability matrix from the so-called *information-matrix* that is composed by the correlation functions of input and output data. To determine the observability matrix, one can start by obtaining the matrices of input-output correlation data.

Given the observability matrix, the system matrix **A.** Modal parameters of the structural system can be estimated by solving the eigenvalues problem of system matrix A. by solving the eigenvalues problem of estimated system matrix to obtain the natural frequency (ω_0) and modal damping ratio (ξ) and mode-shape matrices. Detail information on the system identification algorithm and example of application is given in reference [12].

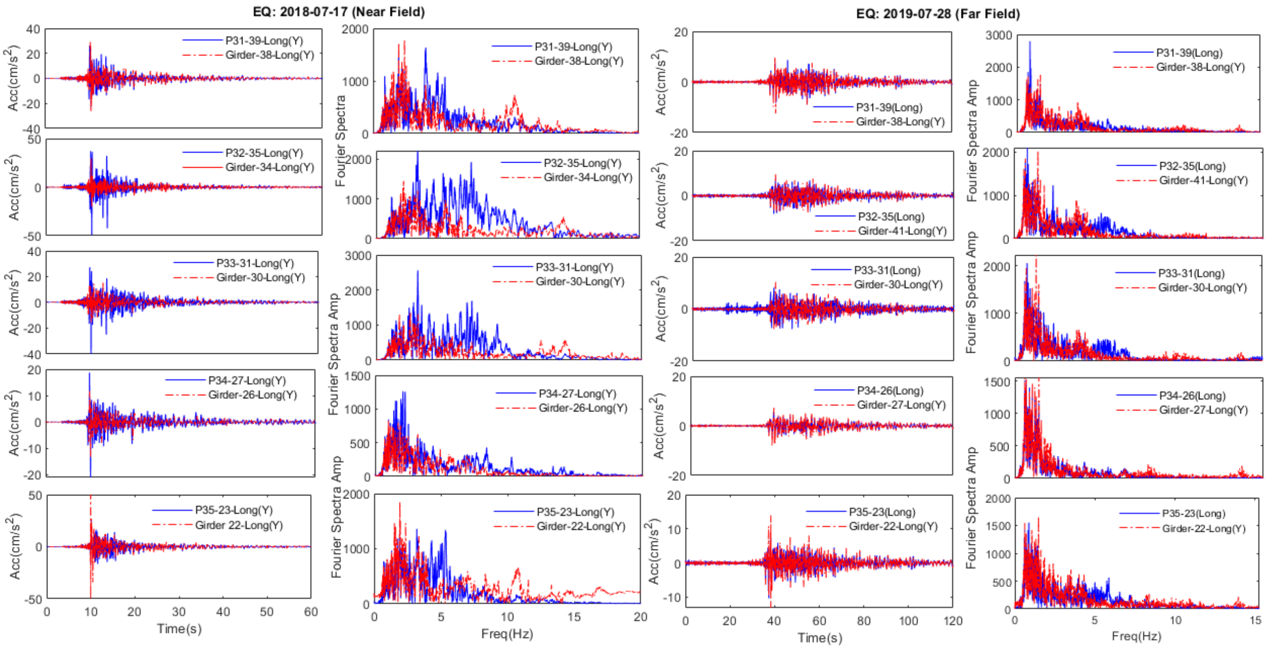

Fig. 8- Comparisons of longitudinal pier-girder accelerations and their frequency characteristics during the nearfield largest earthquake (July 17th ,2018) and far-field largest earthquake (July 28th 2019).

In the system identification, modal parameters of the structural system are estimated. For implementation of the system identifications, the base motion responses recorded by sensor numbers 41,37,33,29,53 and 25 are used as inputs. Whereas all structure accelerations from 20 sensors on the pylon and girders are used as the output. This gives the 6 inputs, 20 outputs in the multi-input multi-output system identification.

For the system identifications, modal parameters are assumed to remain constant during a specific time-window where the data set is analyzed. However, considering the possible non-linear responses of the building during large excitation, the assumption may not be satisfied throughout the whole responses. Therefore, a piece-wise linear analysis was conducted using shorter moving time window (frame), during which the modal parameters were assumed to remain constant. The total time history responses were divided into several frames consisting of 60 seconds of input and output data that each generates a set of modal parameters. Application of the method has been demonstrated to identify modal parameters of long-span bridges in previous works [13].

The system identification method was implemented for all recorded earthquakes. In this paper, examples of the results were shown for the earthquake on July 29th, 2019. This is because, this earthquake provides one of most complete data sets for all sensors with good quality of responses. The results of system identification are listed in Table 2 and compared with the results from finite element model. Shapes of the first two vertical modes are shown in Fig.9. The results from system identification are found sufficiently closed with the finite element and the mode shapes are also relatively close with the results from finite element. Note that the damping values vary depending on the amplitude of earthquake. In the case of seismic responses from July 29th, 2019 earthquake, the modal damping ratios for low order modes are about 2-5% depending on the modes

Table 1 –Identified modal parameters of Shin-Nakagawa Bridge from seismic records on July 29th, 2019.

Mode	Frequency (Hz)	
	Identified from Seismic Records	Finite Element Analysis
1st Vertical	0.356	0.369
1st Longitudinal	0.435	0.410
1st Lateral	0.462	0.442
2nd Vertical	0.748	0.696
3rd Vertical	1.046	1.048
4th Vertical	1.270	1.293

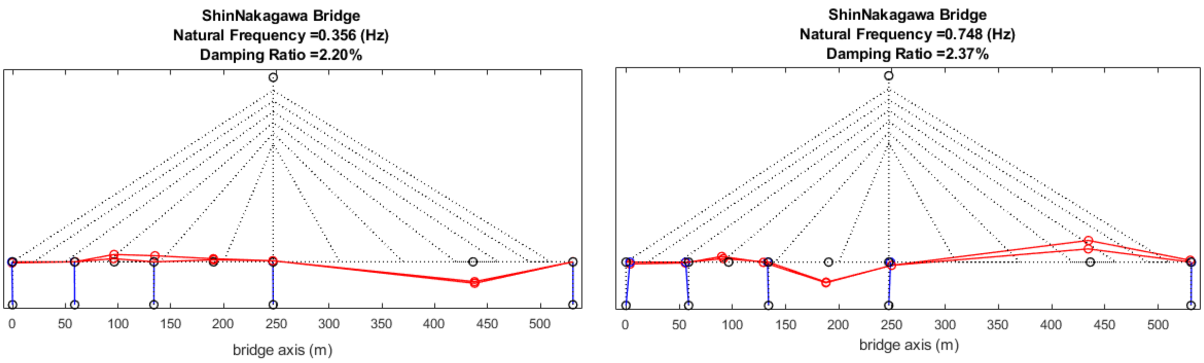

Fig. 9- Example of the first two vertical mode-shapes of Shin-Nakagawa Bridge identified from seismic records on July 29th, 2019.

Frequency spectra of the vertical accelerations recorded by sensors located on the girder between the piers are shown in Fig.9 for the July 29th, 2019 earthquake. It is evident from the figures that the responses were dominated by peaks with frequencies lower than 3Hz. The peaks on frequency spectra correspond well with the modal frequencies identified from system identification (Table 2). Modal parameters of long-span bridge, such as this cable-stayed bridge identified from seismic records may vary depending on the level of seismic excitation as shown in many studies in literature. The sources of variation may come from type of modes, mechanism of energy dissipation and the effective boundary conditions during an earthquake. In case of the Shin-Nakagawa bridge, the various types of bearings connecting the girder and piers provide different mechanisms of energy dissipation as well as boundary condition. With the increase in database from recorded earthquake by wireless sensors, we can evaluate behavior of the bridge and observe the trend in modal parameters and find the relationship between the trend with structural conditions. Detailed study on the effect of bearings and boundary conditions caused by different level of seismic excitation is a topic of an undergoing study.

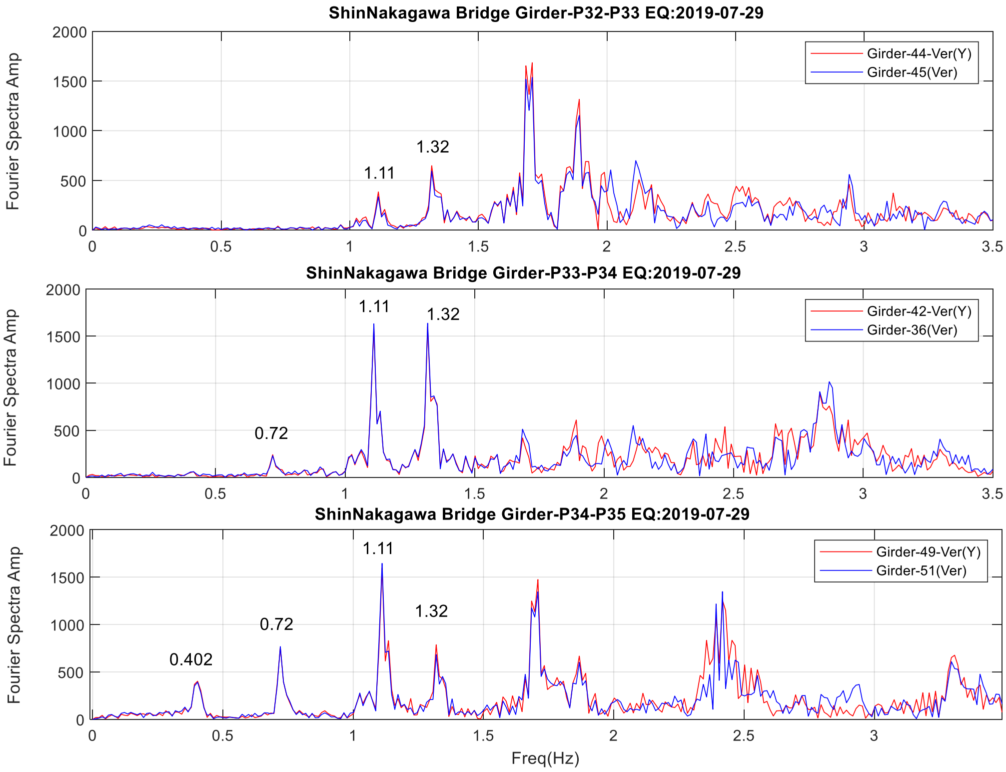

Fig. 10- Frequency spectra of vertical accelerations recorded from girder nodes.

6. Conclusion

This paper describes an ongoing research work on the seismic monitoring of cable-stayed bridge using densely array WSN. The cable-stayed bridge responses have been recorded continuously for more than two years now. The system has successfully recorded more than twenty small-to-moderate-scale earthquakes and from both near-field and far-field earthquake with reasonable accuracy and robustness. Until December 2019, only moderate level of earthquake has been recorded on the bridge, with the largest one having peak ground acceleration of 130cm/s^2.

Based on the series of recorded structural responses, the characteristics of girder and pier vibration were studied. One of the objectives of monitoring is to evaluate performance of seismic isolation bearings between girder and piers. Results observed from the largest earthquake indicate that the seismic isolation bearing has effectively decoupled the superstructure from the substructure. Characteristics of seismically isolated bridge responses, such as high frequency filtering effect and decoupling effect of girder responses can be clearly observed from the records during the largest earthquake.

Multi-input multi-output time-domain system identification was implemented. Natural frequency, modal damping ratios and mode-shapes of the bridge can be identified accurately. In the further study, effect of bearings and boundary conditions caused by different level of seismic excitation will be investigated in more detailed by structural modeling and comparison with structural responses.

8. Acknowledgements

We would like to acknowledge the full support and cooperation from East Nippon Expressway Co., Ltd. East NEXCO Japan in conducting this research. Opinions and findings in the paper are of the authors and not of the abovementioned institution.

9. References

[1] Nagayama T, Spencer Jr BF. (2007): Structural health monitoring using smart sensors. *Newmark Structural Engineering Laboratory. University of Illinois at Urbana-Champaign*.

[2] Cho S, Yun CB, Lynch JP, Zimmerman AT, Spencer Jr BF, Nagayama T. (2008): Smart wireless sensor technology for structural health monitoring of civil structures. Steel Structures, 8(4), 267-275.Park R, Gamble WL (2000): *Reinforced Concrete Slabs*. Wiley, 2nd edition.

[3] Nagayama T, Moinzadeh P, Mechitov K, Ushita M, Makihata N, Ieiri S, Agha G, Spencer Jr BF, Fujino Y, Seo J. (2010): Reliable multi-hop communication for structural health monitoring. *Smart Structures and Systems*. 6(5-6), 481-504

[4] Rice JA, Mechitov K, Sim SH, Nagayama T, Jang S, Kim R, Fujino Y. (2010): Flexible smart sensor framework for autonomous structural health monitoring. *Smart Structures and Systems*, 6(5-6): 423-438.

[5] Jang S, Jo H, Cho S, Mechitov K, Rice JA, Sim SH, Agha G. (2010): Structural health monitoring of a cable-stayed bridge using smart sensor technology: deployment and evaluation. *Smart Structures and Systems*, *6*(5-6), 439-459.

[6] Cho S, Jo H, Jang S, Park J, Jung HJ, Yun CB, Seo JW. (2010): Structural health monitoring of a cable-stayed bridge using wireless smart sensor technology: data analyses. *Smart Structures and Systems*, 6(5-6), 461-480.

[7] Suzuki M, Jinno K, Tashiro Y, Katsumata Y, Liao CH, Nagayama T, Morikawa H. (2016): Development and field experiment of routing-free multi-hop wireless sensor network for structural monitoring. *Proc. ICSIC*, 179-184.

[8] Takahashi, Y. (2011). Damage of rubber bearings and dampers of bridges in 2011 Great East Japan Earthquake. In *Proceedings of the international symposium on engineering lessons learned from* the 2011 Great East Japan Earthquake, March 1-4, 2012, Tokyo, Japan. 1332-1341

[9] http://www.kyoshin.bosai.go.jp/kyoshin/quake/index_en.html (accessed Feb 15th, 2020)

[10] Chaudhary MTA, Abe M, Fujino Y, Yoshida J. (2000): System identification of two base-isolated bridges using seismic records. *Journal of Structural Engineering ASCE*, *126*(10), 1187-1195.

[11] Fujino Y, Siringoringo DM, Kikuchi M, Kasai K, Kashima T. (2019): Seismic Monitoring of Seismically Isolated Bridges and Buildings in Japan—Case Studies and Lessons Learned. *In Seismic Structural Health Monitoring* Springer, Cham; 407-447

[12] Siringoringo DM, Fujino Y. (2008): System identification applied to long-span cable-supported bridges using seismic records. *Earthquake Engineering & Structural Dynamics*, *37*(3), 361-386.

[13] Siringoringo DM, Fujino Y. (2018): Seismic response of a suspension bridge: Insights from long-term full-scale seismic monitoring system. *Structural Control and Health Monitoring*, *25*(11), e2252.1-25

